ACCEPTED MANUSCRIPT

This is the author's peer reviewed, accepted manuscript. However, the online version of record will be different from this version once it has been copyedited and typeset.

Journal of Vacuum Science & Technology A

PLEASE CITE THIS ARTICLE AS DOI: 10.1116/6.0003541

Impact of vacuum ultraviolet photons on ultrathin polymethylmethacrylate during plasma etching

Shikhar Arvind,[1,2] Esben W Larsen,[2] Philippe Bezard,[2] John Petersen,[2] and Stefan De Gendt[1,2]
[1)] *KU Leuven, Celestijnenlaan 200f, 3001 Leuven, BE*
[2)] *imec, Kapeldreef 75, 3001 Leuven, BE*

(*Electronic mail: shikhar.arvind@imec.be)

(Dated: 18 March 2024)

State-of-the-art extreme ultraviolet lithography requires the use of ultrathin photoresists (or resists) due to pattern stability concerns and reduced depth of focus of the extreme ultraviolet lithography scanners. Current resists for extreme ultraviolet lithography are less than 50 nm thick. These ultrathin resists further complicate pattern transfer as unintended plasma-induced damage during dry etching is more pronounced. A better understanding of the interaction of plasma species with ultrathin resists is critical for enabling pattern transfer of sub 10 nm features. Here, we study the impact of vacuum ultraviolet photons, argon ions, and argon plasma on a 40 nm thick polymethylmethacrylate film. Using a deuterium lamp, an industrial ion beam etch tool, and an industrial inductively coupled plasma etch tool, we exposed the polymer to photons, ions, and plasma respectively. The exposed samples were then analyzed for chemical and physical changes using different characterization techniques. It was observed that the vacuum ultraviolet photons interact with the entire bulk of polymer film, while the ions only affect the surface and subsurface region. The photon exposed samples formed smaller polymer fragments at low exposure doses and further started to crosslink at high doses. In contrast, the ion modification lead to carbonization of only the top few nanometers of the polymer film, leaving the bottom bulk intact. The plasma exposed sample showed changes characteristic to both vacuum ultraviolet photons and ions, and their synergism. It was stratified with a (1.34 ± 0.03) nm thick ion-caused carbonized layer on top of (13.25 ± 0.12) nm photon-induced crosslinked layer. By studying the impact of plasma photons on ultrathin polymethylmethacrylate, we were able to establish a baseline for a testing methodology that can be extended to novel ultrathin resist platforms.

I. INTRODUCTION

Extreme ultraviolet lithography (EUV) lithography can now pattern lines with 12 nm half pitch[1]. Patterning of such aggressive pitches requires the use of ultrathin (<50 nm) resists. There are two main reasons for this. Firstly, a typical aspect ratio (height/width) of 2:1 is prescribed to avoid pattern collapse of lines in the resist. As the width of the line decreases for a given thickness, the aspect ratio also increases and with it, the risk of pattern collapse. Secondly, is the reduction of depth of focus (DOF). The current EUV lithography tools have a numerical aperture (NA) of 0.33 and the next generation, high-NA tools are designed with a NA of 0.55. DOF is inversely proportional to square of NA as given by the Rayleigh equation[2], so the DOF is ≈3 times smaller for High NA EUV lithography. Imaging simulations of High NA EUV lithography show that the DOF can be less than 50 nm at narrow pitches[3,4]. Hence, moving to high NA EUV lithography further requires the use ultrathin resists for successful imaging and printing.

Post lithography, the patterned resist serves as a mask for further pattern transfer via plasma etching. One of the main challenges of using ultrathin resists is the reduction of the etch budget during pattern transfer. This is mainly due to more pronounced plasma-induced damage in ultrathin resists. Currently, multiple intermediate hard masks are used to circumvent this, but this makes pattern transfer significantly more complicated and expensive. Understanding the interaction of plasma with ultrathin resists can provide critical insights to aid the development of next generation lithography and pattern transfer processes.

During plasma etch, the direct impact of ions is typically limited to the first few nanometers of polymer whereas the plasma photons can diffuse much deeper into the polymer[5,6]. The vacuum ultraviolet (VUV) photons generated in a cold plasma are of particular interest for us. They have energies between 6 eV to 12 eV and are significant in number[7]. Thus, they can excite and break the polymer bonds, causing considerable modification of the resist. Previous studies have mainly looked at the impact of VUV plasma photons on resists for 193 nm and 248 nm lithography[8–14]. An excellent review of these is covered by Oehrlein *et al*[15]. Pargon *et al*[16,17] and Titus *et al*[18] have also investigated the smoothing effect on the pattern roughness by VUV plasma photons in 193 nm resists. Since these studies focused on older lithography systems, the resists used were relatively thick (>50 nm). There have only been a few studies investigating the interaction of VUV plasma photons with ultrathin resists for EUV lithography[19–22]. The interaction effects of plasma species are expected to be more pronounced in these ultrathin resists and polymers. The top ion-modified layer can itself become a sizable portion of the resist film, while a significant number of VUV photons can penetrate the entire film and further affect the layer below. Furthermore, the influence of the substrate on polymer dynamics and etch rate[23–25] can also be magnified as majority of the bulk is in close proximity to the substrate. The relaxation dynamics, including the glass transition temperature and inter-diffusion mobility, can vary significantly between the free surface and the bottom bulk depending on the nature of polymer-substrate interaction[26].

Two main categories of resists are being developed for EUV

Journal of Vacuum Science & Technology A

ACCEPTED MANUSCRIPT

This is the author's peer reviewed, accepted manuscript. However, the online version of record will be different from this version once it has been copyedited and typeset.
PLEASE CITE THIS ARTICLE AS DOI: 10.1116/6.0003541

lithography : Chemically amplified resists (CARs) and non-CARs. Currently, the most popular class of EUV resists are the CARs, originally developed for deep ultraviolet patterning. A typical EUV CAR has three main components: a main polymer backbone, a photo-acid generator (PAG) and a quencher[27]. The effect of these components' chemistry and their loadings on the plasma-resist interactions is still little known. Additionally, newer non-CAR resists with novel chemistry, such as metal-oxide based resists, are also being explored for low NA EUV and high NA EUV lithography, where they have shown to be promising candidates for the smallest feature sizes at reasonable sensitivity[27,28]. Nevertheless, the interaction of VUV plasma photons with these novel materials is also relatively unexplored.

Polymethylmethacrylate (PMMA) is a widely studied polymer across different fields with relatively simple chemistry. It is used as an open-source photoresist[29], and it is primarily deployed for electron beam (e-beam) lithography. It has also been shown to resolve 50 nm pitch line-space (LS) patterns using EUV lithography[30]. For these reasons, it serves as the ideal starting material to study the impact of plasma species on ultrathin resists. In addition to this, it offers a common baseline for future evaluations of novel polymers and resists.

In this study, we examine the effects of VUV photons and argon ions (Ar^+) on a 40 nm thick PMMA film. By employing a VUV deuterium lamp, an industrial ion beam etch (IBE) tool, and an industrial inductively coupled plasma (ICP) etch tool, we are able to individually process the polymer with VUV photons, ions, and plasma, respectively. This approach enables us to not only isolate the impacts of ions and photons on PMMA, but also explore their combined effects when present in plasma. Using ellipsometry and atomic force microscopy (AFM), we study the thickness and surface roughness changes resulting from the processing. We also wash the samples with two different solvents to characterize the amount of scissioned, pristine-like, crosslinked or carbonized regions within each sample. We further inspect the chemical changes induced during processing using Fourier Transform Infrared spectroscopy (FTIR) and X-ray Photoelectron Spectroscopy (XPS). Based on the observed results, we propose a multilayer ellipsometry model to quantify chemically different layers in the samples. Finally, we conclude by discussing the possible interaction mechanisms of photons and Ar^+ ions with PMMA, and their synergism in Ar plasma.

II. EXPERIMENTAL SETUP

A. Inductively coupled plasma etch tool

A industrial 300 mm ICP source (Lam Research *Kiyo*®) operating at 13.56 MHz was used for Ar plasma exposure of the samples. The source power was set to 1000 W and the pressure was 10 mTorr. No bias was applied.

B. VUV Photon Lamp

A deuterium lamp (Hamamatsu L12542) was used for VUV photons exposure . The on-target stabilized flux of the lamp was estimated using a 1 cm^2 Si photodiode (Opto Diode Corp AXUV100G). This diode efficiently detects a wide range of photon wavelengths (10 nm to 1000 nm). The contribution of high wavelength (>350 nm) photons from the lamp was removed by measuring the current with and without glass (NBK-7) window. The corrected current was converted to power using responsivity curve from diode supplier. The responsivity value at 160 nm was used to calculate the flux as the deuterium lamp spectra peaks at this wavelength. Since responsivity is a function of wavelength, and the lamp is not monochromatic, the flux calculated is an approximation.

C. Ion beam etch tool

A commercial 300 mm IBE tool (IBE-NX , *ANELVA*™ platform by Canon) using remote Ar plasma was used to expose Ar^+ ions on the samples. The lowest possible ion energy setting on the wafer is 50 eV. An ion current of 400 mA was measured for a full 300 mm wafer exposure.

III. SAMPLE PREPARATION

Pristine PMMA (Allresist AR-P 672.01) was spin-coated on a 300 mm Si wafer at 1300 rpm followed by a soft bake at 150 °C for 180 s. The nominal thickness of this film was 40 nm as measured by ellipsometry. The wafer was then diced into coupons (or samples).

These samples were processed under three different processing conditions labeled as: **PHOTONS**, **IONS**, and **PLASMA**.

The PHOTONS samples were exposed with the VUV Deuterium Lamp. The IONS samples were exposed in the Ar IBE tool. The PLASMA samples were exposed in the ICP etch tool. A 40 s processing time was chosen for the PLASMA samples. The Ar plasma parameters were chosen to maximize the generation of VUV photons[31]. The exposure times for the PHOTONS and IONS samples were further adjusted to match the thickness of the PLASMA samples. Hence, all the processed samples were between 15 nm to 17 nm. Due to limited plasma diagnostics available on the industrial ICP tool, exact matching of the photon and ion dose from the plasma was not possible. Instead, by matching the thickness, we could emulate a pure VUV photon etch, a pure ion etch, and a photon-rich plasma etch. The details of the processing conditions are described in Table I.

ACCEPTED MANUSCRIPT
Journal of Vacuum Science & Technology A
This is the author's peer reviewed, accepted manuscript. However, the online version of record will be different from this version once it has been copyedited and typeset.
PLEASE CITE THIS ARTICLE AS DOI: 10.1116/6.0003541

TABLE I. Processing information

Processing name	Sample size	Processing conditions	Processing time(s)	Energy dose ($mJ\,cm^{-2}$)	Film thickness(nm)
Unprocessed	-	-	-	-	39.68 ± 0.08
PHOTONS	2 cm x 2 cm	VUV Lamp, Pressure = 10 mTorr (primary vacuum), Working Distance≈30 cm.	1800	800	16.41 ± 0.77
IONS	3 cm x 3 cm Attached to a Si carrier wafer (300 mm).	IBE tool, Ion energy = 50 eV (lowest possible setting) Pressure = 5×10^{-5} Pa .	53	1240	16.99 ± 0.22
PLASMA	3 cm x 3 cm Attached to a Si carrier wafer (300 mm).	ICP etch tool, Ar plasma, No bias, Source power = 1000 W, Pressure = 10 mTorr.	40	-	15.03 ± 0.06

IV. RESULTS AND DISCUSSION

A. Exposure events in PMMA

Before we discuss the results of various exposures on PMMA, we briefly describe typical changes that occur in irradiated PMMA . There are three phenomena that mainly occur: ***scissioning***, ***crosslinking***, and ***carbonization***. Scissioning refers to the breaking of the polymer main chain into smaller fragments. Crosslinking refers to the formation of chemical bonds between different polymer chains or fragments. This is accompanied by a modest increase in volumetric and optical density compared to pristine polymer. Carbonization refers to the formation of dense amorphous carbon (a-C) like layer. This is caused due to excessive dehydrogenation and deoxygenation of the polymer. In some literature, it is also termed as graphitization[18,32]. Carbonized (or graphitized) films are extremely dense and have a high refractive index (n > 2) compared to pristine films.

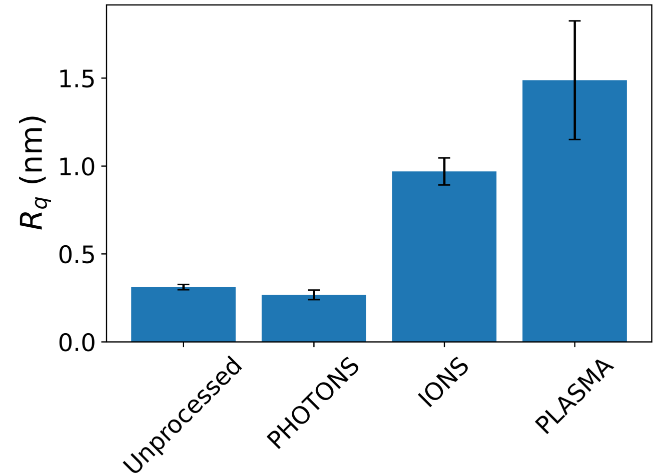

FIG. 1. RMS roughness R_q for different samples measured via AFM.

B. Surface roughness

Figure 1 shows the root-mean-square (RMS) surface roughness R_q for different processing conditions as obtained by atomic force microscopy (AFM). For each processing condition, R_q values were determined from separate locations on multiple samples. The nominal value is the mean of R_q values, and the error is the standard deviation. See supplementary material at [URL will be inserted by AIP Publishing] for more details on AFM characterization.

R_q of the unprocessed samples was 0.3 nm, indicating good spin coat quality. PHOTONS samples' roughness decreased only slightly compared to the unprocessed samples. This suggests that the photon etch is primarily a bulk phenomenon with no surface specific modification. In contrast, both the IONS and PLASMA samples showed a significant increase in R_q. This is due to the Ar^+ ions (present both in IONS and PLASMA processing) that change the surface of polymer significantly.

The PLASMA sample's surface also has larger bubble-like features on surface compared to grainy fine features on the ION sample's surface. See supplementary material at [URL will be inserted by AIP Publishing] for the AFM surface scans of the samples. The presence of these larger features was also confirmed by the radial power spectral desnsity (PSD) of the surface scans. The presence of these bubble-like features on the PLASMA sample can be explained by the synergistic behavior of photons and ions in plasma. Photons interact with the bulk of the film generating volatile by-products. Concurrently the ions are modifying film's surface. These volatile products generated by photons ascend to top and get trapped in the ion modified layer leading to the formation of large bubble-like features on the surface. A similar bubble-like surface topography was observed by Koval *et al*[33] during IBE of e-beam exposed PMMA.

ACCEPTED MANUSCRIPT
Journal of Vacuum Science & Technology A
This is the author's peer reviewed, accepted manuscript. However, the online version of record will be different from this version once it has been copyedited and typeset.
PLEASE CITE THIS ARTICLE AS DOI: 10.1116/6.0003541

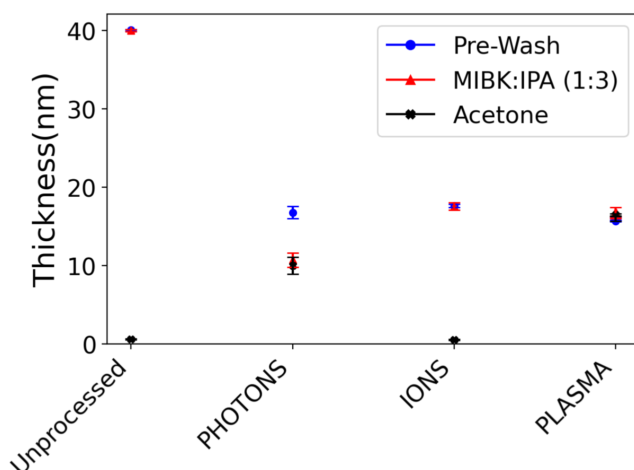

FIG. 2. Thickness (as measured by single-layer model ellipsometry) of different samples after successive washing with MIBK: IPA, followed by acetone.

C. Solvent wash

To get a better understanding of the bulk changes in the samples, they were successively washed with two different solvents. The first solvent was methyl isobutyl ketone (MIBK) diluted with isopropyl alcohol (IPA) at a ratio of 1:3. This is a popular developer for positive tone PMMA lithography. It preferentially dissolves low molecular weight scissioned PMMA fragments[34–36] over pristine, crosslinked, and carbonized PMMA. The second solvent was acetone. It is a stronger solvent of PMMA compared to MIBK:IPA as it dissolves pristine PMMA along with smaller fragments, leaving behind only crosslinked and carbonized polymer[33,37]. The thickness before and after each wash was measured using ellipsometry. Results of one sample for each processing condition is shown in Figure 2. See supplementary material at [URL will be inserted by AIP Publishing] for more details on ellipsometry modelling.

For the unprocessed sample, washing with MIBK:IPA did not change the thickness, indicating that it does not dissolve pristine PMMA. Further washing it with acetone did dissolve the entire layer, confirming the expected behaviour of the solvents. For the PHOTON sample, a $\approx 6\,\mathrm{nm}$ reduction in processed film thickness was observed after washing with MIBK:IPA. This indicates that photons cause some scissioning creating smaller polymer fragments which were washed by MIBK:IPA. Further, washing the sample with acetone did not change the thickness appreciably. Hence, the remaining $\approx 10\,\mathrm{nm}$ of sample, which is the larger fraction, is either crosslinked or carbonized. Additionally, it was observed that at lower dose exposures($\approx 400\,\mathrm{mJ\,cm^{-2}}$, not shown here) the entire film is washed away by MIBK:IPA. This means that at low doses of the photon exposure, PMMA is mainly scissioned, but beyond a certain threshold dose, the polymer starts to gradually crosslink. Similar behavior has been observed with electron beam exposure on PMMA[37].

For the IONS sample, no scission products were detected as the thickness did not change after washing with MIBK:IPA. This further means that surface change observed via AFM must be due to either crosslinking or carbonization. Further washing the sample with acetone dissolved the entire film. This reveals the presence of pristine-like PMMA in the bottom of the film. The entire film can be washed away even if a few nanometers at the bottom is pristine-like, as the top cannot adhere to the substrate.

Finally, for the PLASMA sample, neither of the solvents changed the thickness appreciably. This indicates that both the surface and bulk are either crosslinked or carbonized.

V. IR SPECTROSCOPY

To further analyze bulk chemistry changes, IR spectra of the samples were collected using attenuated total reflection (ATR) Fourier transform infrared spectroscopy (FTIR). See supplementary material at [URL will be inserted by AIP Publishing] for more details on ATR-FTIR setup.

There are three important regions with peaks corresponding to different stretching vibrations in PMMA : C=O ($1730\,\mathrm{cm^{-1}}$), C−O−C ($1240\,\mathrm{cm^{-1}}$) and C−H ($2800\,\mathrm{cm^{-1}}$). The IR spectra of these regions is plotted in Figure 3. The presence of clear C−O−C peak is a useful indicator for the presence of pristine-like PMMA. This is because the ester side chain is quite labile and its decarboxylation is a dominant reaction during degradation of PMMA[30].

The PHOTONS and PLASMA samples show notable decrease in peak area of the C=O region relative to the unprocessed sample, while the C−H peak did not exhibit as significant a relative decrease. This indicates that the reduced peak intensity in these samples is not only due to a thinner film but also due to additional chemical changes leading to significant deoxygenation. This is further highlighted by almost no C−O−C peak showing almost complete side chain degradation. The C−H region for these samples also shows a shift in the peak position compared to the unprocessed sample suggesting the formation of new carbon bonds, likely via photon-induced crosslinking. In contrast, the IONS sample shows all the peaks seen in the unprocessed sample including the C−O−C peak, albeit at a lower intensity. The lower intensity is due to a thinner film and some additional chemical changes at the surface due to Ar^+ ions. The presence of C−O−C peak indicates the presence of considerable pristine-like PMMA in the bulk, reaffirming the results from the solvent wash test.

VI. REFRACTIVE INDEX

Refractive index $n(\lambda)$ values obtained from the ellipsometry of the samples are plotted as a function of wavelength in Figure 4. As explained in Section IV A, by comparing the $n(\lambda)$ value, we can further discern between crosslinking and carbonization in the processed samples.

The IONS sample showed the highest increase in $n(\lambda)$. From the solvent wash and IR spectra results it is known

ACCEPTED MANUSCRIPT
Journal of Vacuum Science & Technology A
This is the author's peer reviewed, accepted manuscript. However, the online version of record will be different from this version once it has been copyedited and typeset.
PLEASE CITE THIS ARTICLE AS DOI: 10.1116/6.0003541

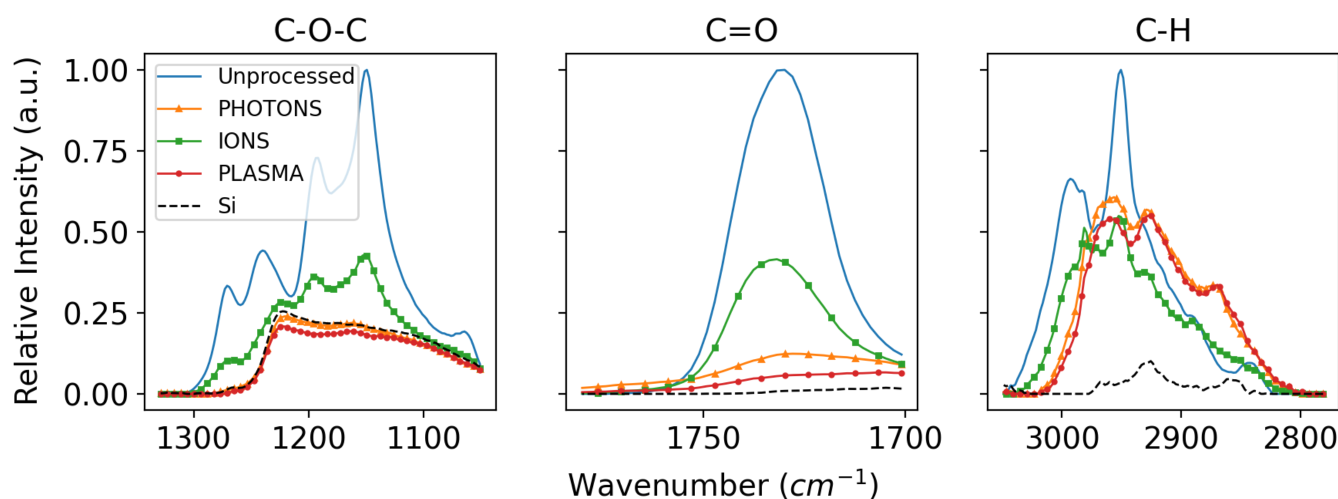

FIG. 3. Relative IR absorbance spectra of vibrations corresponding to relevant regions of different samples including bare Silicon. The C-O-C and C=O peaks decrease significantly in PHOTONS and PLASMA samples due to photon-induced deoxygenation. The IONS sample has decreased peak area but still retain the peaks corresponding to pristine-like PMMA. See supplementary material at [URL will be inserted by AIP Publishing] for full the IR spectra.

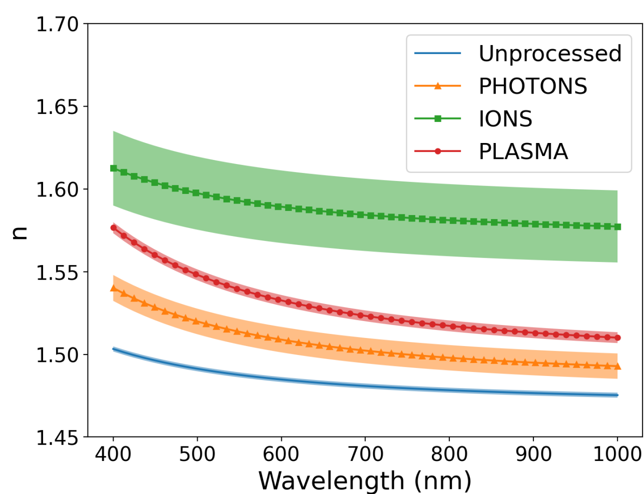

FIG. 4. Refractive index $n(\lambda)$ of different samples as measured by the single-layer ellipsometry model. The solid line is the mean $n(\lambda)$ while the shaded area is the standard deviation.

317 that these samples have considerable pristine-like PMMA in
318 the bulk with mainly the surface/subsurface region modified.
319 Thus, the change in the refractive index with respect to un-
320 processed sample must be from this top ion modified layer.
321 The significant jump in $n(\lambda)$ hints at the formation of a dense
322 carbonized layer. Additonally, as we move from the surface
323 to the subsurface region, the energy deposited by the ions de-
324 creases. Hence, a transition from the dense carbonized surface
325 to a crosslinked subsurface region, and finally to a pristine-like
326 bulk, is expected[33].

327 The PHOTONS sample showed a modest increase in $n(\lambda)$.
328 From the solvent wash results, we know that a smaller frac-
329 tion of this sample is scissioned while the larger fraction is
330 either crosslinked or carbonized. It was observed that scis-
331 sioning caused negligible change in $n(\lambda)$, indicating that the
332 main change in $n(\lambda)$ for this sample must originate from the
333 crosslinked or carbonized region. If the larger fraction were
334 carbonized, we would expect $n(\lambda)$ to be higher than IONS
335 sample, which is not the case. Conversely, crosslinking typ-
336 ically leads to a modest increase in $n(\lambda)$[38], as is seen in this
337 sample. Hence, the major fraction of PHOTONS sample is
338 determined to be crosslinked and not carbonized.

339 The PLASMA sample exhibits a considerable increase in
340 $n(\lambda)$, though it still falls short compared to the IONS sample.
341 A similar argument can be made as in the case of the PHO-
342 TONS sample that the undissolved bulk in the PLASMA sam-
343 ple is crosslinked and not carbonized. Additionally, drawing
344 from the IONS results, a carbonized ion modified layer at the
345 surface is also expected due to the ions in the plasma. If this
346 ion modified layer were congruent with that of the IONS sam-
347 ple, then the PLASMA sample would show the highest $n(\lambda)$,
348 surpassing the IONS sample. Evidently it does not, hence the
349 ion modification is not equivalent in the two cases.

350 There are two reasons for this. Firstly, the ion bombard-
351 ing energy in the ICP tool is lower than that in IBE tool.
352 Typical Ar^+ ion energy in an ICP with no bias is 15 eV to
353 20 eV[39] , whereas the ion energy during IBE was 50 eV.
354 Lower ion energy leads to a shallower range of ions in the
355 PLASMA sample[40], leading to a thinner carbonized layer.
356 Secondly, the total energy deposited of the ions is also dif-
357 ferent between the two. Higher ion doses can increase the
358 degree of carbonization[41] and, in some cases the thickness of
359 the carbonized layer too[42,43]. Thus, the ion modification in
360 the PLASMA sample is weakly carbonized compared to the
361 IONS sample.

Journal of Vacuum Science & Technology A

ACCEPTED MANUSCRIPT

This is the author's peer reviewed, accepted manuscript. However, the online version of record will be different from this version once it has been copyedited and typeset.

PLEASE CITE THIS ARTICLE AS DOI: 10.1116/6.0003541

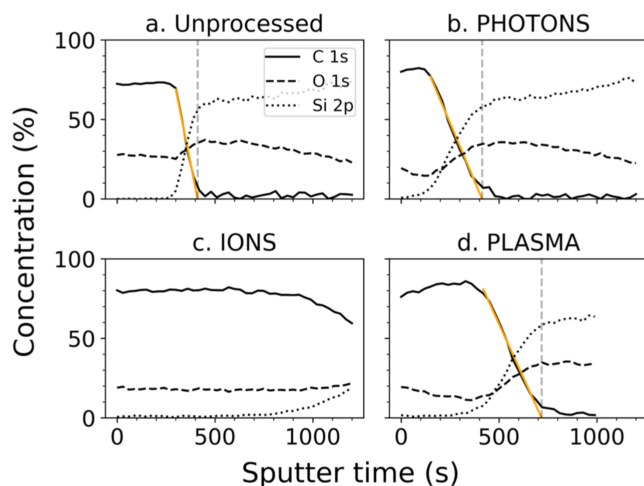

FIG. 5. C 1s , O 1s and Si 2p atomic concentrations as depth profiles from XPS for a. Unprocessed sample , b. PHOTONS sample, c. IONS sample and d. PLASMA sample. The sputter clear time (vertical dashed line) is calculated as the x intercept of the decreasing C 1s rate (orange line). The IONS sample was not fully cleared within 1200s.

VII. X-RAY PHOTOELECTRON SPECTROSCOPY

To develop a better understanding of chemical changes throughout the film, a XPS depth profile measurement was performed on all the samples. A monochromatized photon beam of Al K_α line (1486.6 eV) along with a Ar gas cluster ion beam (GCIB) as the sputter beam was used. The cluster size was 1000 atoms with an energy of 2.5 eV / atom. Ar GCIB was used as it causes minimal polymer damage during sputtering[44]. The sputter duration was limited to $<$1200 s . See supplementary material at [URL will be inserted by AIP Publishing] for more details on the XPS setup and spectra analysis.

The C 1s, O 1s and Si 2p atomic concentrations from the depth profile for different samples are plotted in Figure 5. In addition to these elements, trace amounts of N and Br were also detected in the IONS and PLASMA samples due to contamination of the chamber walls of the IBE and ICP tools. For the depth profile, we define the sputter clear time as the total time to clear the entire sample polymer. It depends on both the thickness and chemical resistance of the layer. It was calculated by finding the x-intercept of the decreasing slope of C 1s as shown by the dashed line in Figure 5. Since the thicknesses of processed samples are similar, differences in their total sputter time are mainly due to chemical variations between them.

The IONS sample did not clear within 1200 s due to the carbonized layer at the top. Inorganic materials, like amorphous carbon layers, have a significantly lower GCIB sputter rate compared to polymers[45]. Due to the extremely low sputter rate of the top carbonized layer, the probed region also moves very slowly during the initial $\approx$ 800 s leading to minimal change in the atomic concentrations. Closer inspection of the variation of the O 1s spectra at different sputter times further confirms the presence of a buried pristine-like layer. With increasing sputter time, a high binding energy (BE) peak shoulder($\approx$ 533.5 eV) emerges and subsequently disappears for the O 1s spectra. See supplementary material at [URL will be inserted by AIP Publishing] for the O 1s spectra at different sputter times. This behavior can only be attributed to the O−C peak from the buried pristine-like layer, as the O=C peak is present at a lower BE ($\approx$ 531 eV) and the O−Si peak contribution from the substrate is expected to either increase or saturate with increasing sputter times.

The PHOTONS sample has a comparable sputter clear time as the unprocessed sample even with it being less than half the thickness of the unprocessed sample. This improved sputter resistance is due to the crosslinked region in the sample. For the PLASMA sample, the sputter clear time is higher than PHOTONS but less than that of IONS. The increased sputter clear time relative to PHOTONS sample is due to a combination of slightly thicker crosslinked layer and the presence of an weakly carbonized layer at the top.

The PHOTONS and PLASMA samples also exhibit an interesting trend of increasing relative C/O ratio deeper into the sample. A similar C/O trend was seen for even low dose photon exposed samples , implying that this behavior is characteristic of photon exposed PMMA ultrathin films. A possible mechanism for this is proposed by considering the process of photon-induced outgassing and the transport of molecules in polymer thin films.

During initial exposure, VUV photons attack the polymer leading to the formation of free radicals. These radicals stabilize by forming volatile molecules and smaller fragments leading to scissioning of the polymer. Ho *et al*[46] performed outgassing studies on PMMA thin films exposed to VUV photons. They observed that most of the outgassed fragments were large molecules like $C_5H_8O_2$, C_3H_4O, CH_3OH and CH_2O. The diffusivity of molecules in polymers decreases significantly with their molecular size[47]. These large volatile molecules formed at at the top can easily escape as they have to diffuse less before desorbing from the film surface. Conversely, the same volatile molecules formed at the bottom in the film cannot outgas as quickly due to a longer diffusion process to reach the surface. As the sample is continually exposed to photons, these deeper volatile molecules can undergo further photodegradation, forming more free radicals and smaller volatile products like CO or CO_2 which eventually outgas. Crosslinking occurs at increasing doses of photon exposure due to the increasing density of radicals, raising the probability of reactions between fragments, similar to high dose exposures of e-beam on PMMA[29,37]. The larger volatile molecules outgassing from the top are more carbon rich than the smaller molecules outgassing from the bottom. Hence, the top loses relatively more carbon than at the bottom leading to the observed C/O trend in XPS depth profile.

ACCEPTED MANUSCRIPT
Journal of Vacuum Science & Technology A
This is the author's peer reviewed, accepted manuscript. However, the online version of record will be different from this version once it has been copyedited and typeset.
PLEASE CITE THIS ARTICLE AS DOI: 10.1116/6.0003541

TABLE II. Thickness of the characteristic layers from the multi-layer model for each sample. The total thickness from the multi-layer and single layer model is also tabulated for each sample. The values 0 correspond to disabled fit of that layer as fitting it would give negative thickness value of the same.

Sample	**Single-layer**	**Multi-layer**			
	Total (nm)	Pristine/Scissioned (nm)	Crosslinked (nm)	Carbonized (nm)	*Total (nm)*
Unprocessed	39.68 +/- 0.08	39.26 +/- 0.16	0.3 +/- 0.14	0	39.56 +/- 0.30
PHOTONS	16.41 +/- 0.77	5.73 +/- 0.94	10.46 +/- 0.24	0	16.19 +/- 1.18
IONS	16.99 +/- 0.22	11.94 +/- 1.31	2.52 +/- 1.29	3.09 +/- 0.15	17.55 +/- 2.7
PLASMA	15.03 +/- 0.06	0	14.28 +/- 0.1	1.21 +/- 0.12	14.59 +/- 0.15

VIII. MULTI-LAYER ELLIPSOMETRY MODEL

Based on the previous results, we propose a multi-layer ellipsometry model to further quantify the thicknesses of chemically different layers within the processed samples. The model includes three different characteristic layers with fixed optical constants: ***Pristine-like/Scissioned***, ***Crosslinked*** and ***Diamond-like-carbon (DLC)***.

For accounting pristine and scissioned PMMA, an identical characteristic layer was used as minimal difference was observed between their optical constants. The optical constants for this layer were obtained by fitting a Cauchy absorbent layer for an unprocessed sample. For crosslinked layer, the optical constants were obtained by fitting a PHOTONS sample washed with acetone as this sample only has photon-induced crosslinked polymer remaining (refer Figure 2). Finally, to account for the carbonized layer due to ions, a DLC layer was used. DLC is a class of a-C with relatively more sp^3 than sp^2 hybridization[48]. Its optical constants vary depending on the density, type of hybridization and the amount of hydrogen in the film[49]. Since the exact composition of the carbonized layer was not known, a Tauc-Lorentz oscillator model representing a DLC was obtained from the tool CompleteEASE™software database. See supplementary material at [URL will be inserted by AIP Publishing] for the optical constants of the three characteristic layers. The order of the layer stacking is also different for these samples. For all the samples, the DLC layer is on the top. For the unprocessed and IONS samples, the crosslinked layer is above the pristine/scissioned layer and for PLASMA and PHOTONS samples it is the vice-versa.

The results from the multi-layer model is shown in Figure 6. To evaluate the multi-layer model, the total thickness obtained from it is compared to the total thickness from the single-layer model. These values are tabulated in Figure 6.

For the PHOTONS samples, the total thickness from the multi-layer model is statistically identical to that of the single-layer model. We obtain a $\approx 5.7\,\text{nm}$ scissioned layer with the rest of the film crosslinked. This is also in good agreement with the thickness difference observed from the solvent wash (Figure 2). For the IONS sample, the multi-layer total thickness is slightly higher than the single-layer value. The thickness of the DLC layer is (3.09 ± 0.15) nm. Molecular dynamic (MD) simulations of $100\,\text{eV}$ Ar^+ on PMMA by Choudry *et al*[50] reported the steady state thickness of carbonized layer to be $\approx 2\,\text{nm}$. The overestimation of thickness

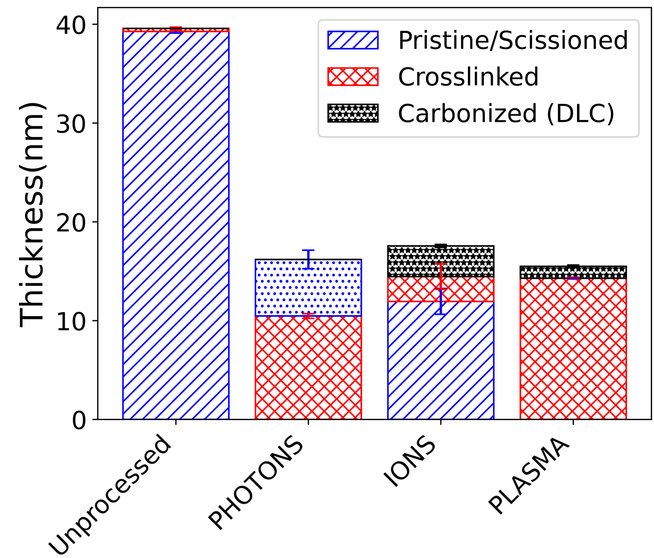

FIG. 6. Thickness of different characteristic layers for different samples using the multi-layer ellipsometry model.

in our model is due to DLC layer used. If the actual carbonized layer has higher $n(\lambda)$ and $k(\lambda)$ than the DLC, then the thickness of the carbonized layer during fitting can be overestimated. This can also explain the slight overestimation of the total thickness compared to the single-layer model.

For the PLASMA sample, the total thickness from the multi-layer model is slightly underestimated compared to single-layer value. In this case, the carbonization at the top is probably lesser than what is modeled by DLC. Additionally, the same crosslinked layer was also used for both PHOTONS and PLASMA samples. As seen from XPS depth profile, the C/O of the PLASMA sample is slightly different compared to the PHOTONS sample. This can further lead to differences between the reported crosslinked layer thickness and the actual value.

IX. INTERACTION MECHANISMS

Computational study by Conforti *et al*[51] showed that VUV photon with wavelengths around $160\,\text{nm}$ have enough energy to cause PMMA degradation via multiple pathways. The polymer can undergo chain scissioning directly via main chain

Journal of Vacuum Science & Technology A

ACCEPTED MANUSCRIPT

This is the author's peer reviewed, accepted manuscript. However, the online version of record will be different from this version once it has been copyedited and typeset.

PLEASE CITE THIS ARTICLE AS DOI: 10.1116/6.0003541

fragmentation or indirectly via first side chain scission which can further lead to main chain fragmentation[30]. This depends on the exact polymer chemistry and the energy of the incident photons[52–54]. Outgassing studies of VUV photon exposure on PMMA have shown that the majority of the outgassed fragments correspond to byproducts of main chain scission[46,54]. Irrespective of the exact fragmentation pathway, at high doses of photon exposure, the density of the photo-generated radicals increases, leading to crosslinking. The VUV photons also penetrate fully into the ultrathin polymer[6]. In contrast to this, Ar^+ ions mainly interact with the surface or near surface region of the polymer. By performing Monte Carlo simulations of 50 eV Ar^+ ions on PMMA using the Stopping and Range of Ions in Matter (SRIM) software package[40], we estimate the mean range of the ions to be less than 3 nm. At such low ion energies, the energy loss is dominated by nuclear stopping. Nuclear stopping refers to the collisions of the impinging ions with the atoms of the target material. It is highly efficient at breaking bonds, causing rapid degassing and further carbonization[55] as discussed above. If a target atom at the surface has enough energy from the ion collision cascade to overcome the surface binding energy, it can also sputter away leading to ion sputtering[40,56].

Plasma is a complex system where various species interact synergistically with PMMA. This leads to effects that are not observed in individual exposures. In the previous sections, we have elucidated the synergistic effects of photons and ions in Ar plasma on ultrathin PMMA. The ion induced carbonized layer is expected to form within the first few seconds of plasma exposure[14,15]. Similarly, the VUV photons induced scissioning is also expected to begin at initial plasma exposure in PMMA. Since crosslinking needs a high concentration of radicals and thus a threshold dose of VUV photons, it takes relatively longer to establish. This further depends on the photon energy, flux, and synergistic effects in plasma. From our results, we observed some initial crosslinking of PMMA already at the shortest exposure time of 10 s in Ar plasma. Heating also has been reported to play an important role in the synergistic effects with VUV photons on 193 nm resists[57]. Due to limitations in the current testing setup, the synergistic effects of heating and VUV photons were not examined in this study. Electrons and metastable Ar neutrals[58] present in the plasma can also cause additional polymer modification.

X. CONCLUSION

Modification of ultrathin PMMA under VUV photons, Ar^+ ions, and Ar plasma was investigated. The Ar^+ ion impacted only the top of the polymer film, creating the ion-modified layer. This ion-modified layer was stratified, with carbonization at the top followed by a transitory crosslinked layer. Conversely, VUV photons interacted with the entire bulk of the polymer. At low photon doses, only scissioning of the main chain was observed. At higher doses, due to the increased density of free radicals in the film, crosslinking was detected. Additionally, from the XPS depth profiles of the photon exposed samples, an increasing C/O ratio deeper into the film was detected. A possible mechanism was proposed based on differences in the composition and diffusivity of outgassed products at the surface compared to the bottom. In Ar plasma, the synergistic effects of photons and ions were observed. The surface showed bubble-like features which was attributed to the trapping of photon-generated volatile molecules in the top ion-modified layer. The bulk was also photo-induced crosslinked with an increasing C/O ratio towards the bottom as in the case of only VUV photon exposed sample. The extent of carbonization and crosslinking within the various processed samples was calculated using a multi-layer ellipsometry model.

ACKNOWLEDGEMENT

The authors acknowledge funding from the imec Industrial Affiliation Program (IIAP). Shikhar Arvind acknowledges funding from KU Leuven for their doctoral studies. The authors would like to thank Shreya Kundu of imec for their help with IBE tool. The authors would also like to thank Materials Characterization and Analysis (MCA) group at imec for their help with AFM and XPS analysis.

AUTHOR DECLARATION

A. CONFLICT OF INTEREST

The authors declare no conflict of interest.

B. AUTHOR CONTRIBUTIONS

Shikhar Arvind: Conceptualization (equal); Investigation (lead); writing – original draft (lead); formal analysis (lead); writing – review and editing (equal) **Esben W Larsen:** Conceptualization (equal); Investigation (equal); formal analysis (supporting); Supervision (equal); writing – review and editing (equal) **Philippe Bezard:** Conceptualization (equal); Investigation (equal); formal analysis (supporting); Supervision (equal); writing – review and editing (equal) **John Petersen:** Conceptualization (equal); Investigation (equal); formal analysis (supporting); Supervision (equal); writing – review and editing (equal) **Stefan De Gendt:** Conceptualization (equal); Investigation (equal); formal analysis (supporting); Supervision (equal); writing – review and editing (equal)

DATA AVIALABILITY

The data that support the findings of this study are available from the corresponding author upon reasonable request.

[1] X. Wang, L.-T. Tseng, T. Allenet, I. Mochi, M. Vockenhuber, C.-K. Yeh, L. van Lent-Protasova, J. G. Santaclara, R. Custers, and Y. Ekinci,

ACCEPTED MANUSCRIPT

Journal of Vacuum Science & Technology A

This is the author's peer reviewed, accepted manuscript. However, the online version of record will be different from this version once it has been copyedited and typeset.
PLEASE CITE THIS ARTICLE AS DOI: 10.1116/6.0003541

"Progress in EUV resists status towards high-NA EUV lithography," in *Extreme Ultraviolet (EUV) Lithography XI*, Vol. 11323 (SPIE, 2020) pp. 56–66.

[2] C. Mack, *Fundamental Principles of Optical Lithography: The Science of Microfabrication*, 1st ed. (Wiley, 2007).

[3] E. Van Setten, G. Bottiglieri, J. McNamara, J. Van Schoot, K. Troost, J. Zekry, T. Fliervoet, S. Hsu, J. Zimmermann, M. Roesch, B. Bilski, and P. Graeupner, "High NA EUV lithography: Next step in EUV imaging," in *Extreme Ultraviolet (EUV) Lithography X*, edited by K. A. Goldberg (SPIE, San Jose, United States, 2019) p. 5.

[4] A. Burov, A. Vaglio Pret, and R. Gronheid, "Depth of focus in high-NA EUV lithography: A simulation study," in *Photomask Technology 2022*, edited by B. S. Kasprowicz and T. Liang (SPIE, Monterey, United States, 2022) p. 46.

[5] M. J. Titus, D. G. Nest, and D. B. Graves, "Modelling vacuum ultraviolet photon penetration depth and C=O bond depletion in 193 nm photoresist," Journal of Physics D: Applied Physics **42**, 152001 (2009).

[6] M. Fouchier, E. Pargon, L. Azarnouche, K. Menguelti, O. Joubert, T. Cardolaccia, and Y. C. Bae, "Vacuum ultra violet absorption spectroscopy of 193 nm photoresists," Applied Physics A **105**, 399–405 (2011).

[7] D. Popović, M. Mozetič, A. Vesel, G. Primc, and R. Zaplotnik, "Review on vacuum ultraviolet generation in low-pressure plasmas," Plasma Processes and Polymers **18**, 2100061 (2021).

[8] D. Nest, T.-Y. Chung, D. B. Graves, S. Engelmann, R. L. Bruce, F. Weilnboeck, G. S. Oehrlein, D. Wang, C. Andes, and E. A. Hudson, "Understanding the Roughening and Degradation of 193 nm Photoresist during Plasma Processing: Synergistic Roles of Vacuum Ultraviolet Radiation and Ion Bombardment," Plasma Processes and Polymers **6**, 649–657 (2009).

[9] R. L. Bruce, S. Engelmann, T. Lin, T. Kwon, R. J. Phaneuf, G. S. Oehrlein, B. K. Long, C. G. Willson, J. J. Végh, D. Nest, D. B. Graves, and A. Alizadeh, "Study of ion and vacuum ultraviolet-induced effects on styrene- and ester-based polymers exposed to argon plasma," Journal of Vacuum Science & Technology B: Microelectronics and Nanometer Structures **27**, 1142 (2009).

[10] M. J. Titus, D. G. Nest, T.-Y. Chung, and D. B. Graves, "Comparing 193 nm photoresist roughening in an inductively coupled plasma system and vacuum beam system," Journal of Physics D: Applied Physics **42**, 245205 (2009).

[11] D. Nest, T.-Y. Chung, J. J. Végh, D. B. Graves, R. L. Bruce, T. Lin, R. J. Phaneuf, G. S. Oehrlein, B. K. Long, and C. G. Willson, "Role of polymer structure and ceiling temperature in polymer roughening and degradation during plasma processing: A beam system study of P4MS and PαMS," Journal of Physics D: Applied Physics **43**, 085204 (2010).

[12] F. Weilnboeck, R. L. Bruce, S. Engelmann, G. S. Oehrlein, D. Nest, T.-Y. Chung, D. Graves, M. Li, D. Wang, C. Andes, and E. A. Hudson, "Photoresist modifications by plasma vacuum ultraviolet radiation: The role of polymer structure and plasma chemistry," Journal of Vacuum Science & Technology B, Nanotechnology and Microelectronics: Materials, Processing, Measurement, and Phenomena **28**, 993–1004 (2010).

[13] T.-Y. Chung, D. B. Graves, F. Weilnboeck, R. L. Bruce, G. S. Oehrlein, M. Li, and E. A. Hudson, "Ion and Vacuum Ultraviolet Photon Beam Effects in 193 nm Photoresist Surface Roughening: The Role of the Adamantyl Pendant Group," Plasma Processes and Polymers **8**, 1068–1079 (2011).

[14] F. Weilnboeck, N. Kumar, G. S. Oehrlein, T.-Y. Chung, D. Graves, M. Li, E. A. Hudson, and E. C. Benck, "Real-time measurements of plasma photoresist modifications: The role of plasma vacuum ultraviolet radiation and ions," Journal of Vacuum Science & Technology B, Nanotechnology and Microelectronics: Materials, Processing, Measurement, and Phenomena **30**, 031807 (2012).

[15] G. S. Oehrlein, R. J. Phaneuf, and D. B. Graves, "Plasma-polymer interactions: A review of progress in understanding polymer resist mask durability during plasma etching for nanoscale fabrication," Journal of Vacuum Science & Technology B, Nanotechnology and Microelectronics: Materials, Processing, Measurement, and Phenomena **29**, 010801 (2011).

[16] E. Pargon, M. Martin, K. Menguelti, L. Azarnouche, J. Foucher, and O. Joubert, "Plasma impact on 193 nm photoresist linewidth roughness: Role of plasma vacuum ultraviolet light," Applied Physics Letters **94**, 103111 (2009).

[17] E. Pargon, L. Azarnouche, M. Fouchier, K. Menguelti, R. Tiron, C. Sourd, and O. Joubert, "HBr Plasma Treatment Versus VUV Light Treatment to Improve 193 nm Photoresist Pattern Linewidth Roughness," Plasma Processes and Polymers **8**, 1184–1195 (2011).

[18] M. J. Titus, D. B. Graves, Y. Yamaguchi, and E. A. Hudson, "Effects of vacuum ultraviolet photons, ion energy and substrate temperature on line width roughness and RMS surface roughness of patterned 193 nm photoresist," Journal of Physics D: Applied Physics **44**, 085204 (2011).

[19] P. De Schepper, Z. el Otell, A. Vaglio Pret, E. Altamirano-Sanchez, and S. De Gendt, "The Influence of H2 Plasma Treatment on LWR Mitigation: The Importance of EUV Photoresist Composition," Plasma Processes and Polymers **12**, 624–641 (2015).

[20] P. De Schepper, A. Vaglio Pret, Z. el Otell, T. Hansen, E. Altamirano-Sanchez, and S. De Gendt, "Pattern Roughness Mitigation of 22 nm Lines and Spaces: The Impact of a H2 Plasma Treatment," Plasma Processes and Polymers **12**, 153–161 (2015).

[21] A. Pranda, K.-Y. Lin, S. Engelmann, R. L. Bruce, E. A. Joseph, D. Metzler, and G. S. Oehrlein, "Significance of plasma-photoresist interactions for atomic layer etching processes with extreme ultraviolet photoresist," Journal of Vacuum Science & Technology A **38**, 052601 (2020).

[22] A. Pranda, *Plasma-Photoresist Interactions for Realizing Advanced Pattern Transfer Processes*, Ph.D. thesis, University of Maryland (College Park, Md.) (2020).

[23] N. Vourdas, A. G. Boudouvis, and E. Gogolides, "Plasma etch rate measurements of thin PMMA films and correlation with the glass transition temperature," Journal of Physics: Conference Series **10**, 405–408 (2005).

[24] G. Cunge, D. Ferrah, C. Petit-Etienne, A. Davydova, H. Okuno, D. Kalita, V. Bouchiat, and O. Renault, "Dry efficient cleaning of poly-methyl-methacrylate residues from graphene with high-density H2 and H2-N2 plasmas," Journal of Applied Physics **118**, 123302 (2015).

[25] D. Marinov, J.-F. De Marneffe, Q. Smets, G. Arutchelvan, K. M. Bal, E. Voronina, T. Rakhimova, Y. Mankelevich, S. El Kazzi, A. Nalin Mehta, P.-J. Wyndaele, M. H. Heyne, J. Zhang, P. C. With, S. Banerjee, E. C. Neyts, I. Asselberghs, D. Lin, and S. De Gendt, "Reactive plasma cleaning and restoration of transition metal dichalcogenide monolayers," npj 2D Materials and Applications **5**, 17 (2021).

[26] B. Li, S. Zhang, J. S. Andre, and Z. Chen, "Relaxation behavior of polymer thin films: Effects of free surface, buried interface, and geometrical confinement," Progress in Polymer Science **120**, 101431 (2021).

[27] T. Manouras and P. Argitis, "High Sensitivity Resists for EUV Lithography: A Review of Material Design Strategies and Performance Results," Nanomaterials **10**, 1593 (2020).

[28] G. Lim, K. Lee, S. Choi, and H. J. Yoon, "Organometallic and coordinative photoresist materials for EUV lithography and related photolytic mechanisms," Coordination Chemistry Reviews **493**, 215307 (2023).

[29] F. Rahman, D. J. Carbaugh, J. T. Wright, P. Rajan, S. G. Pandya, and S. Kaya, "A review of polymethyl methacrylate (PMMA) as a versatile lithographic resist – With emphasis on UV exposure," Microelectronic Engineering **224**, 111238 (2020).

[30] A. Rathore, I. Pollentier, H. Singh, R. Fallica, D. D. Simone, and S. D. Gendt, "Effect of molecular weight on the EUV-printability of main chain scission type polymers," Journal of Materials Chemistry C **8**, 5958–5966 (2020).

[31] J. B. Boffard, C. C. Lin, C. Culver, S. Wang, A. E. Wendt, S. Radovanov, and H. Persing, "Comparison of surface vacuum ultraviolet emissions with resonance level number densities. I. Argon plasmas," Journal of Vacuum Science & Technology A: Vacuum, Surfaces, and Films **32**, 021304 (2014).

[32] I. Lazareva, Y. Koval, M. Alam, S. Strömsdörfer, and P. Müller, "Graphitization of polymer surfaces by low-energy ion irradiation," Applied Physics Letters **90**, 262108 (2007).

[33] Y. Koval, "Mechanism of etching and surface relief development of PMMA under low-energy ion bombardment," Journal of Vacuum Science & Technology B: Microelectronics and Nanometer Structures **22**, 843 (2004).

[34] J. S. Greeneich, "Solubility Rate of Poly-(Methyl Methacrylate), PMMA, Electron-Resist," Journal of The Electrochemical Society **121**, 1669 (1974).

[35] B. Cord, J. Lutkenhaus, and K. K. Berggren, "Optimal temperature for development of poly(methylmethacrylate)," Journal of Vacuum Science & Technology B: Microelectronics and Nanometer Structures Processing, Measurement, and Phenomena **25**, 2013–2016 (2007).

Journal of Vacuum Science & Technology A
ACCEPTED MANUSCRIPT
This is the author's peer reviewed, accepted manuscript. However, the online version of record will be different from this version once it has been copyedited and typeset.
PLEASE CITE THIS ARTICLE AS DOI: 10.1116/6.0003541

[36] M. J. Rooks, E. Kratschmer, R. Viswanathan, J. Katine, R. E. Fontana, and S. A. MacDonald, "Low stress development of poly(methylmethacrylate) for high aspect ratio structures," Journal of Vacuum Science & Technology B: Microelectronics and Nanometer Structures Processing, Measurement, and Phenomena **20**, 2937–2941 (2002).
[37] I. Zailer, J. E. F. Frost, V. Chabasseur-Molyneux, C. J. B. Ford, and M. Pepper, "Crosslinked PMMA as a high-resolution negative resist for electron beam lithography and applications for physics of low-dimensional structures," Semiconductor Science and Technology **11**, 1235–1238 (1996).
[38] W. J. Tomlinson, I. P. Kaminow, E. A. Chandross, R. L. Fork, and W. T. Silfvast, "Photoinduced refractive index increase in Poly(Methylmethacrylate) and its applications," Applied Physics Letters **16**, 486–489 (1970).
[39] D. J. Economou, "Tailored ion energy distributions on plasma electrodes," Journal of Vacuum Science & Technology A: Vacuum, Surfaces, and Films **31**, 050823 (2013).
[40] J. F. Ziegler, J. P. Biersack, and M. D. Ziegler, *SRIM, the Stopping and Range of Ions in Matter* (SRIM Company, 2008).
[41] D. Fink, R. Hull, R. M. Osgood, J. Parisi, and H. Warlimont, eds., *Fundamentals of Ion-Irradiated Polymers*, Springer Series in Materials Science, Vol. 63 (Springer Berlin Heidelberg, Berlin, Heidelberg, 2004).
[42] K. J. Orvek and C. Huffman, "Carbonized layer formation in ion implanted photoresist masks," Nuclear Instruments and Methods in Physics Research Section B: Beam Interactions with Materials and Atoms **7–8**, 501–506 (1985).
[43] P. Gröning, O. Küttel, M. Collaud-Coen, G. Dietler, and L. Schlapbach, "Interaction of low-energy ions (< 10 eV) with polymethylmethacrylate during plasma treatment," Applied Surface Science **89**, 83–91 (1995).
[44] H.-Y. Chang, W.-C. Lin, P.-C. Chu, Y.-K. Wang, M. Sogo, S.-i. Iida, C.-J. Peng, and T. Miyayama, "X-ray Photoelectron Spectroscopy Equipped with Gas Cluster Ion Beams for Evaluation of the Sputtering Behavior of Various Nanomaterials," ACS Applied Nano Materials **5**, 4260–4268 (2022).
[45] M. P. Seah, "Universal Equation for Argon Gas Cluster Sputtering Yields," The Journal of Physical Chemistry C **117**, 12622–12632 (2013).
[46] G. H.-Y. Ho, H.-M. Lin, and C.-Y. Yeh, "Photo-electron chemistry of photoresist outgassing upon DUV, VUV, EUV, and BEUV irradiation," Journal of Photochemistry and Photobiology A: Chemistry **353**, 306–315 (2018).
[47] W.-C. Chen, S.-J. Lee, and B.-C. Ho, "Diffusion coefficients of acrylic monomers in poly(methyl methacrylate)," Journal of Polymer Research **5**, 187–191 (1998).
[48] A. Grill, "Diamond-like carbon: State of the art," Diamond and Related Materials **8**, 428–434 (1999).
[49] X. Zhou, T. Suzuki, H. Nakajima, K. Komatsu, K. Kanda, H. Ito, and H. Saitoh, "Structural analysis of amorphous carbon films by spectroscopic ellipsometry, RBS/ERDA, and NEXAFS," Applied Physics Letters **110**, 201902 (2017).
[50] G. K. Choudhary, J. J. Végh, and D. B. Graves, "Molecular dynamics simulations of oxygen-containing polymer sputtering and the Ohnishi parameter," Journal of Physics D: Applied Physics **42**, 242001 (2009).
[51] P. F. Conforti, Y. G. Yingling, and B. J. Garrison, "Computational studies of ultraviolet ablation of poly(methyl methacrylate)," Journal of Physics: Conference Series **59**, 322–327 (2007).
[52] S. Kueper, S. Modaressi, and M. Stuke, "Photofragmentation pathways of a PMMA model compound under UV excimer laser ablation conditions," The Journal of Physical Chemistry **94**, 7514–7518 (1990).
[53] K. Okudaira, E. Morikawa, S. Hasegawa, P. Sprunger, V. Saile, K. Seki, Y. Harada, and N. Ueno, "Radiation damage of poly(methylmethacrylate) thin films analyzed by UPS," Journal of Electron Spectroscopy and Related Phenomena **88–91**, 913–917 (1998).
[54] N. Ueno, T. Mitsuhata, K. Sugita, and K. Tanaka, "Mechanism of UV- and VUV-Induced Etching of Poly(methyl methacrylate)," in *Polymers in Microlithography*, ACS Symposium Series, Vol. 412 (American Chemical Society, 1989) Chap. 26, pp. 424–436.
[55] V. Kumar, B. Chaudhary, V. Sharma, and K. Verma, eds., *Radiation Effects in Polymeric Materials*, Springer Series on Polymer and Composite Materials (Springer International Publishing, Cham, 2019).
[56] P. Sigmund, "Theory of Sputtering. I. Sputtering Yield of Amorphous and Polycrystalline Targets," Physical Review **184**, 383–416 (1969).
[57] D. Nest, D. B. Graves, S. Engelmann, R. L. Bruce, F. Weilnboeck, G. S. Oehrlein, C. Andes, and E. A. Hudson, "Synergistic effects of vacuum ultraviolet radiation, ion bombardment, and heating in 193nm photoresist roughening and degradation," Applied Physics Letters **92**, 153113 (2008).
[58] A. Bard, K. K. Berggren, J. L. Wilbur, J. D. Gillaspy, S. L. Rolston, J. J. McClelland, W. D. Phillips, M. Prentiss, and G. M. Whitesides, "Self-assembled monolayers exposed by metastable argon and metastable helium for neutral atom lithography and atomic beam imaging," Journal of Vacuum Science & Technology B: Microelectronics and Nanometer Structures Processing, Measurement, and Phenomena **15**, 1805–1810 (1997).